Not available on line

Not available on line

Not available on line

Not available on line

CEFDA04-1218

Task Title: TW5-TVD-HHFT: MONITORING AND ANALYSIS OF DIVERTOR COMPONENTS TESTED IN FE200: 200 kW ELECTRON BEAM GUN TEST

INTRODUCTION

Thermomechanical fatigue is one of the most important damaging mechanism for the Plasma Facing Components (PFC) of the ITER machine due to the high number of operating cycles (several thousands) and to the expected surface heat loads. Therefore an assessment of the behaviour of PFCs under cycling heat loads is essential to demonstrate the fitness for purpose of the selected design solutions. This contract concerns the monitoring and analysis of thermal fatigue testing of PFC to be performed in the frame of the European R&D programme for ITER.

2006 ACTIVITIES

3 testing campaigns were performed at the high heat flux testing FE200 facility [1] during the year 2006.

Mock-up W_monoblock

Description of the mock-up

This component was manufactured by Ansaldo Ricerche by high temperature brazing. It is a straight 27 mm width tungsten (W) monoblock component, with an armoured length of about 300 mm (armour thickness on top is 7.5 mm). The 12/15 mm ID/OD cooling tube is made of CuCrZr (see figure 1).

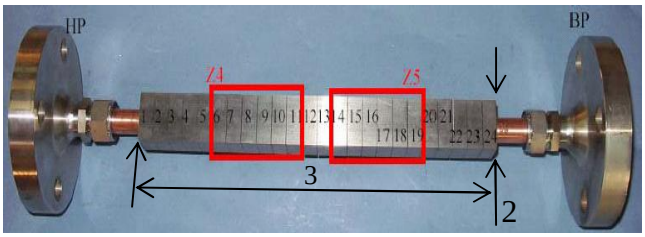

Figure 1: W_monoblock mock-up made of 24 blocs with flanges for FE200 heating – the 2 heating zones Z4 and Z5 are marked in red

High heat flux testing

There was no twisted tape in the cooling channel; therefore the water cooling temperature was reduced down to 50 °C (to be compared with a nominal value of 100-120°C) during high heat flux testing to avoid critical heat flux events. The cooling water conditions at the inlet were 3.5 MPa, 12 m/s. The W heated surfaces were glassblated before testing for emissivity homogenisation.
After a first step of inrared emissivity estimation, it was set at 0.30 for the infrared (IR) analog Inframetrics device (3-5 µm). Imaging under a steady-state flux of 5 MW/m² performed with a reduced range pointed out non-uniform temperature field. However, the range of temperature non-uniformity was limited to 540-680°C (see figure 2) to be compared with a calculation of 640°C: this means that the brazing processes between W and copper were successfull (there is no presence of unexpected thermal resistance).

The following testing steps were performed on 2 zones of 6 blocks named Z4 and Z5, results are given table 1.

Table 1: Description of the testing steps

Testing steps (10 sec. ON / 10 sec. OFF)	Observations
5 MW/m² x 100 cycles	No observed degradation
10 MW/m² x 1000cycles	No observed degradation
20 MW/m² x 1000cycles	Melting of W on the edges of mock-up

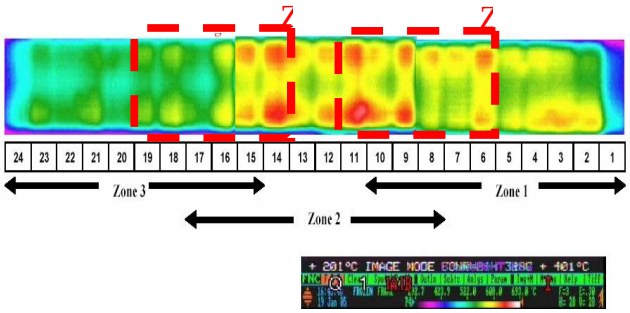

Figure 2: Infrared imaging of the mock-ups under an absorbed steady-state heat flux of 5 MW/m².
Image is to be flipped for comparison with figure 1

Thermal behaviour was stable during the steps at 5 and 10 MW/m². During the first steps at 20 MW/m², experimental surface temperature were consistent with calculations (figure 3).

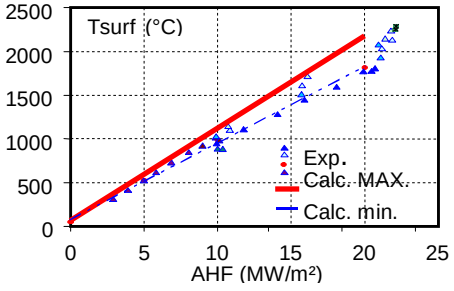

Figure 3: Experimental/calculated surface temperature at steady-state

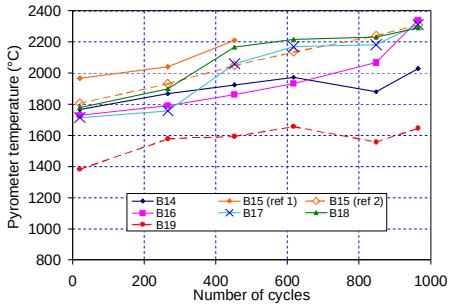

Figure 4: Evolution of steady-state surface temperature during cycling step at 20MW/m²

Continuous increasing of temperature during the step at 20 MW/m² was observed with pyrometers and Infrared device (figure 4). However, calibration and emissivity estimation were performed only up to 1500°c and did not allow quantitative analysis on temperature field (cf [2]). The fatigue step was pursued up to 1000 cycles as foreseen in the testing plan: sides of the mock-up systematically melted during this step (figure 5). It was not possible to detect melting of the W with IR devices during the experiment.

Interpretation

Large debonding between soft copper and W may explain the melting edges: figure 6 shows an ANSYS calculation with implementation of debonding leading to a surface temperature of 3400°C (melting temperature of W). This shows that the high temperature brazing process is not compatible with fluxes of 20 MW/m². Metallographic examination may confirm this assumption.

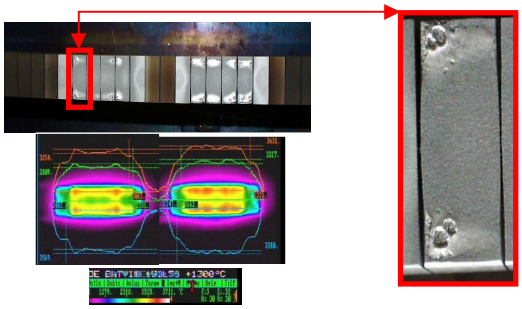

Figure 5: Visual aspect after 1000 cycles at 20 MW/m² and IR image; Zoom on surface

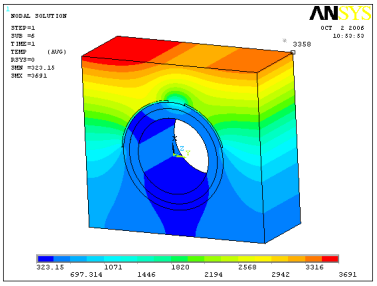

Figure 6: ANSYS model with implementation of bonding for interpretation of melting on the edges (90° on the left, 70° on the right)

Mock-up W_hypervap

Description of the mock-up

Two medium-scale vertical target prototypes were tested. One was manufactured by Plansee via HIP'ing and the other by Ansaldo Ricerche via high temperature brazing. They are both full flat tile vertical target prototypes with W armour and hypervapotron CuCrZr heat sink assembled on SS316L rear plate by explosion bonding (figure 7).

a)

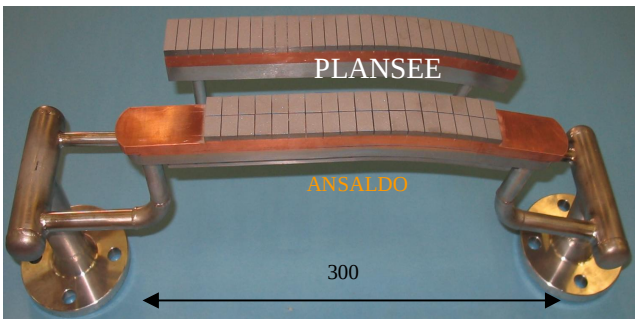

b)

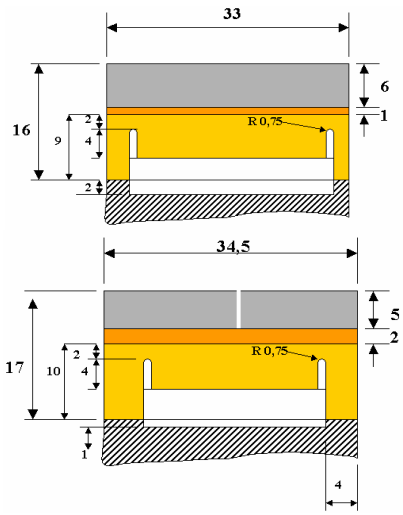

Figure 7: a) The 2 prototypes mounted on a supporting cooled structure for FE200 testing
b) Sketch of the cross sections

High heat flux testing

Table 2: Description of the testing steps

Testing steps (10 sec. ON / 10 sec. OFF)	Observations
5 MW/m² x 100 cycles	No observed degradation
10 MW/m² x 1000cycles	No observed degradation
20 MW/m² x 766 cycles	Overheating of tiles

The cooling water conditions at the inlet were 3.5 MPa, 8 m/s, 100°C. The W heated surfaces were glassblated before testing for emissivity homogenisation.

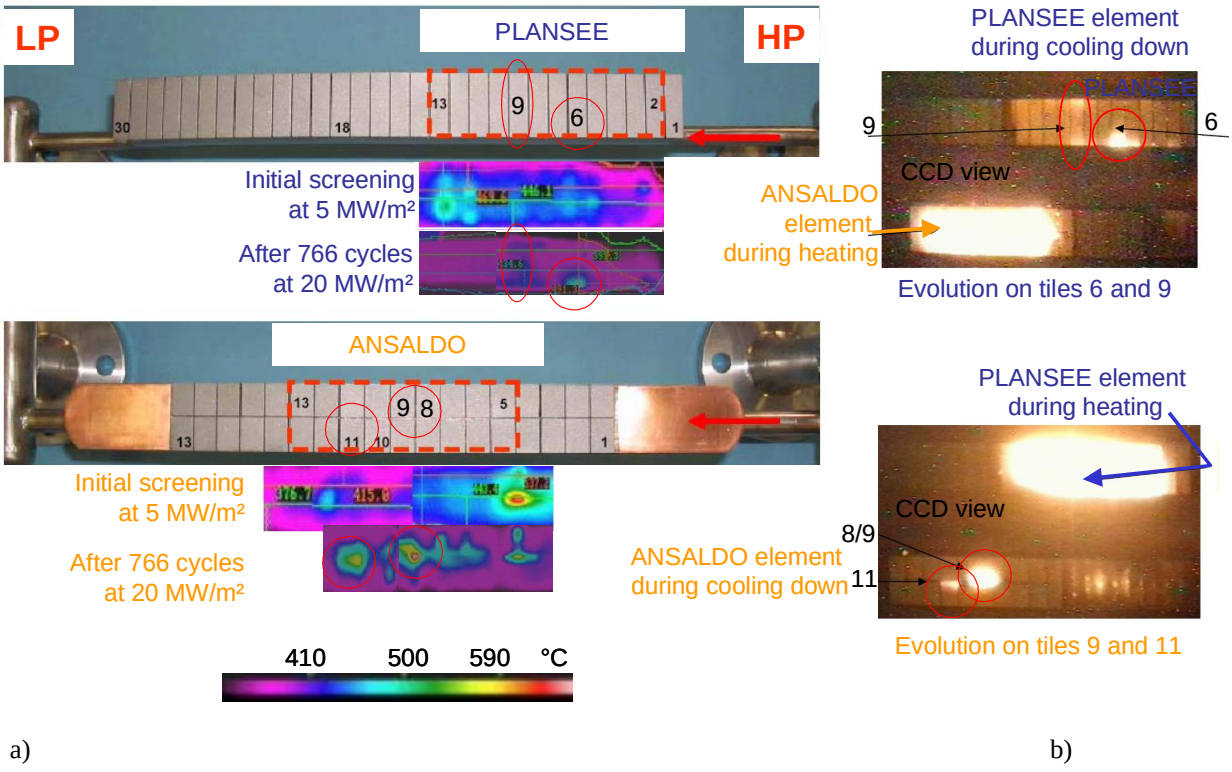

Figure 8: Infrared (a) and visible (b) view of overheated tiles on the prototypes

Figure 8 shows initial and final screening after cycling at 20 MW/m²: the tiles overheated during the step at 20 MW/m² (4 tiles: #6, 9 for Plansee prototype and #8-9, 11 for Ansaldo) were not detected during initial screening (tests are extensively described in [4]. Furthermore, it was detected a global increasing of surface temperature during the step at 20 MW/m² (figure 9).
Finally, it was decided to stop the fatigue testing at this point (dangerous overheating of vacuum chamber due to radiation from hot W).

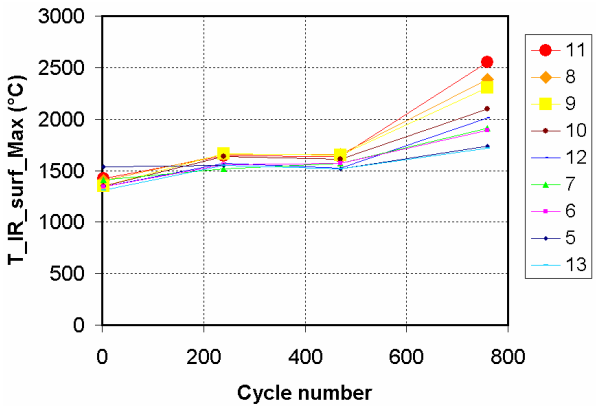

Figure 9: Steady-state temperature under a flux of 20 MW/m² - Global increasing of surface temperature + overheating of tiles #8-9, 11 on Ansaldo prototype

Interpretation

Behaviour of these W components may be explained by a failure mode already observed with CFC armoured flat tile geometry during manufacturing of Tore Supra limiter or W7-X divertor. Above a certain heat flux value, a sudden development of debonding at one of the interfaces may appear after an unpredictable number of cycles. The use of hypervapotron geometry increases the heat flux treshold (typically from 10 MW/m² on smooth tube geometry to 20 MW/m²) but doesn't modify the failure mode. This assumption may be confirmed by metallographic examination on tile 9 of the Ansaldo component where was estimated the propagation of a strip defect of 4-6 mm (figure 10).

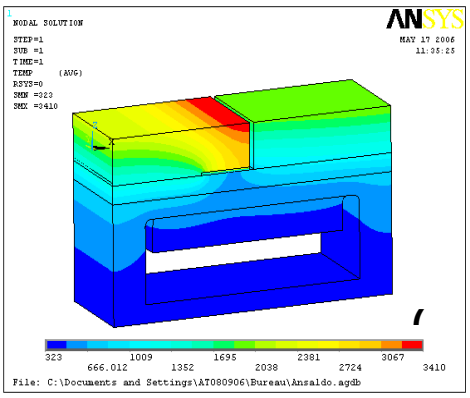

a)

b)

Figure 10: a) Impact of a 6 mm defect on surface temperature for a flux of 20 MW/m²
b) Zoom on T9 surface of Ansaldo prototype

Mock-up HRP

Description of the mock-up

The so-called HRP mock-up is a curved monoblock vertical target prototype made of CFC NB31 and W blocks, CuCrZr tube and SS316L backplate manufactured by ENEA via Pre Brazed Casting (PBC) and Hot Radial Pressing (HRP) patented processes. The high heat flux unit is mounted onto the 316L supporting structure by means of pins of CuCrZr allowing the sliding. A swirl tape - twist ratio 2 - is inserted into the straight part of the CuCrZr tube (figure 11).

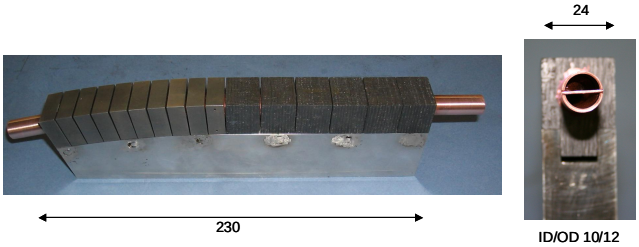

Figure 11: The HRP mock-up

High heat flux testing

Table 3: Description of the testing steps

Testing steps (10 sec. ON / 10 sec. OFF)	Observations
5 MW/m² x 100 cycles	No observed degradation
10 MW/m² x 3000cycles	No observed degradation
20 MW/m² x 2000 cycles on CFC part 15 MW/m² x 2000 cycles on W part	No observed degradation

The cooling water conditions at the inlet were 3.5 MPa, 12 m/s, 100°C. The W heated surfaces were glassblated before testing for emissivity homogenisation. Steps of cycling did not show evolution of surface temperature at 5 and 10 MW/m². At 15/20 MW/m² on W/CFC parts, a small increase was detected (figure 12) without consequence on the heat removal capability of the mock-up. Infrared surface temperature both on W and CFC parts are proposed figure 13.

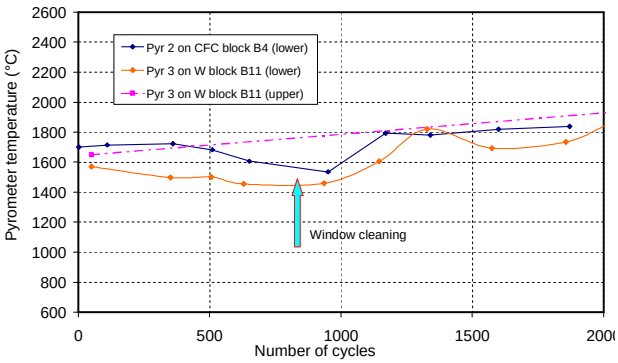

Figure 12: Evolution of surface temperature during cycling step at 15/20 MW/m²

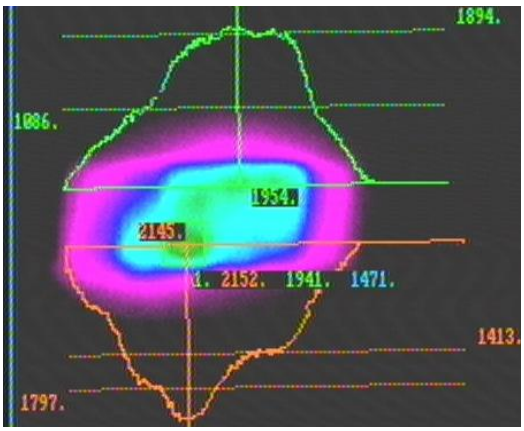

a) W side (B14-B8)

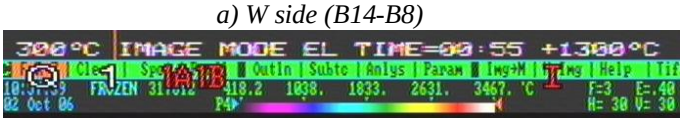

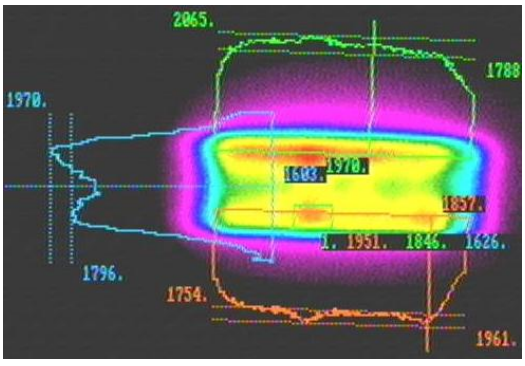

b) CFC side (B5-B2)

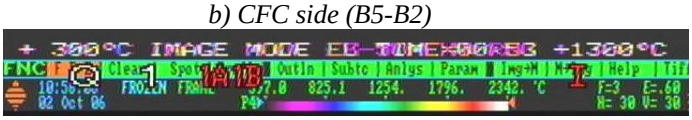

Figure 13: Infrared surface temperature during cycling step at 15/ 20 MW/m²

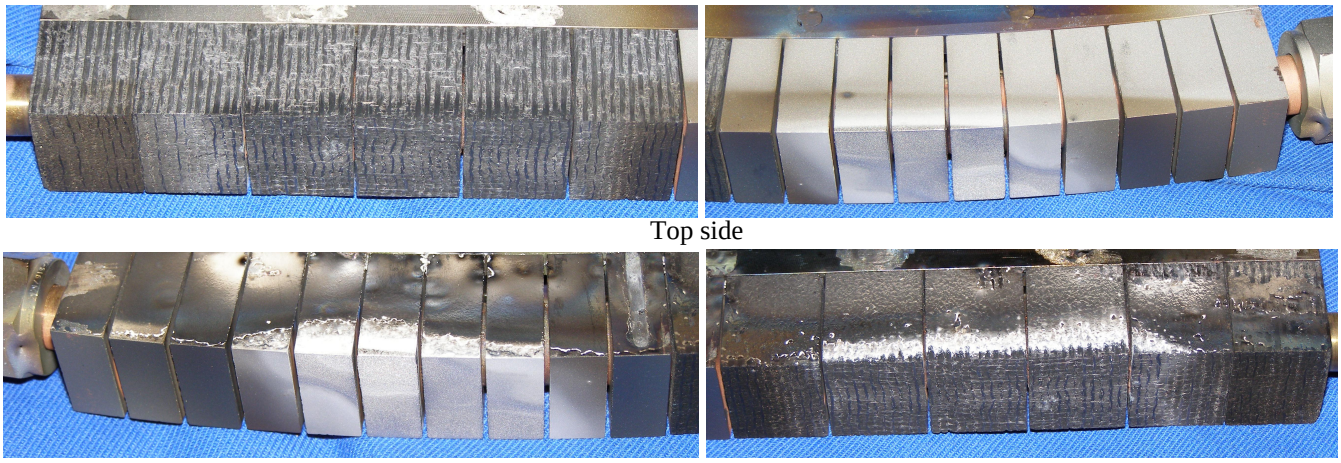

Figure 14: Mock-up aspect after cycling at 15/20 MW/m²

CONCLUSIONS

3 prototypes were high heat flux tested in the frame of this contract at FE200 facilities, the main conclusions are the following:

- High temperature brazing process proposed by Ansaldo Ricerche on W monoblocks is adapted for removal of 10 MW/m² but is not compatible with fluxes of 20 MW/m²;

- The use of hypervapotron heat sink geometry with W flat tile increases the heat flux treshold beyond which failure starts (typically from 10 MW/m² on smooth tube geometry to 20 MW/m²) but doesn't modify the typical flat tile failure mode;

- The Pre Brazed Casting (PBC) and Hot Radial Pressing (HRP) processes patented by ENEA used for W and CFC monoblocks manufacturing shows an excellent behaviour under heat fluxes up to respectively 15 and 20 MW/m² on W and CFC monoblocks.

Activities in the frame of this contract are completed.

REPORTS AND PUBLICATIONS

[1] Fus. Eng. Des. 75-79 (2005) 357-363, I. Bobin- Vastra, F.Escourbiac, M.Merola, P.Lorenzetto

[2] AREVA report NFT- F R-06.928A - CEA89 – EFDA/93-851JN – I.Bobin-Vastra, 2006

[3] Spécifications techniques pour la maquette W_monoblock à tester au FE200 – CFP/NTT- 2006.002, F.Escourbiac, 2006

[4] AREVA report NFT- F R-06.929A – CEA90 – EFDA/93-851JN – I.Bobin-Vastra, 2006

[5] Spécifications techniques pour la maquette W_hypervap à tester au FE200 – CFP/NTT-2006.012, S. Constans, 2006

[6] AREVA report NFT- F R-06.930A – CEA91 – EFDA/93-851JN – I.Bobin-Vastra, 2006

[7] Spécifications techniques pour la maquette HRP à tester au FE200 – CFP/NTT-2006.021, F.Escourbiac, 2006

TASK LEADER

Frédéric ESCOURBIAC

DSM/DRFC/SIPP
CEA-Cadarache
F-13108 Saint-Paul-lez-Durance Cedex

Tel. : 33 4 42 25 44 00
Fax : 33 4 42 25 49 90

e-mail : frederic.escourbiac@cea.fr

CEFDA05-1243

Task Title: TW5-TVD-NDTEST: UPGRADE OF THE SATIR TEST BED FOR INFRARED THERMOGRAPHIC INSPECTIONS – DESIGN PHASE

INTRODUCTION

Among all Non-Destructive Examinations (NDE), active infrared thermography by internal thermal excitation is becoming recognized as a technique available today to improve quality control of many materials and structures involved in heat transfer. The infrared thermography allows to characterise the brazed bond between two materials with different thermal physical properties. An infrared thermography test bed named SATIR (Station Acquisition Traitement Infra Rouge) has been developed by CEA in order to evaluate the manufacturing process quality of actively water-cooled high heat flux components (PFCs) before their installation in Tore Supra. In order to increase the defect detection limit of the SATIR, several possibilities had been assessed in the frame of a previous contract [1]. The installation in 2003 of a digital infrared camera and the improvement of the thermal signal processing, has led to a considerable increase of performances.

In 2001 the main conclusion of the following EFDA contract [1] showed that:

- The increase of temperature range (up to 200°C) would involve complete pressurization of the test bed. Finite element calculations showed that this solution allows a significant improvement of sensitivity (by factor 2) but it was not retained because SATIR would become less flexible in its use (Pressure Safety Standard).
- The implementation in 2003 of a cooled digital IR camera using wavelengths range 3-5mm instead of a scanning infrared camera allowed to develop a new data processing, which led to a significant improvement of performances.
- The increase of water velocity inside the tested component involves an increase of the convective heat transfer coefficient, which improves in a significant way the sensitivity of SATIR diagnostic.

2006 ACTIVITIES

TEST BED DESCRIPTION

The principle of SATIR test (figure 1) is to generate successively a hot and a cold-water front in the cooling channel of the elements, in order to measure the surface temperature evolution.
A cooled infrared digital camera is used to detect zones where heat exhaust is not sufficient. Defects like braze voids are detected by a slower temperature response of the surface during transient. Geometry tolerances and the material properties dispersion play a major role in the determination of acceptance criteria. In case of serial control, two components are tested in parallel with a reference. A DTref criterion is defined with respect to the reference. The detailed principle of SATIR facility and DTref Criterion were subject to many papers [2].

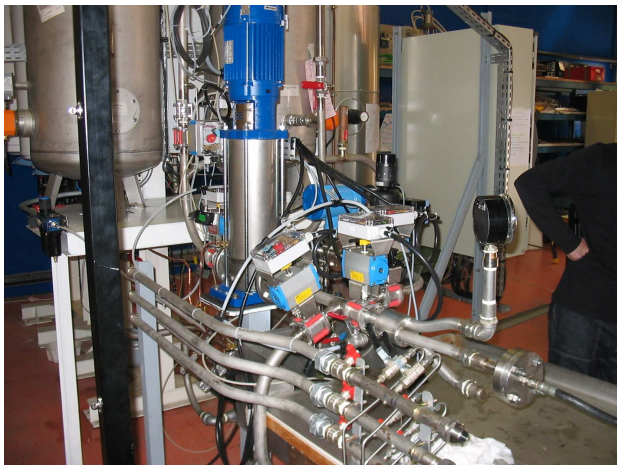

Figure 1: View of SATIR test bed

Within the on-going work on acceptance criteria task, which is being carried out by EU and the ITER International team, SATIR inspection has been identified as the basic test to decide upon the final acceptance of the Divertor PFCs [3]. However, the ITER Divertor PFCs pose new challenges for the following reasons:
The CFC thickness is 2-3 times higher (18-20 mm) than any existing component manufactured or being manufactured so far either within the ITER project or within domestic projects. Therefore, the sensitivity of the technique, which depends on the armour thickness, is lowered.
The number of units to be tested is 2-3 times higher (more than 2000) than on any existing or under construction fusion machine. Therefore, the total time required to test all the units increases accordingly.

This involves, as a consequence, the following needs:

i) To increase the water velocity,
ii) To minimise the test time.

INCREASE OF WATER VELOCITY

To investigate the water velocity effect on the detection sensitivity, a simulation of SATIR experiment by finite element calculations (CAST3M, figure 2) has been carried out on ITER CFC monoblock, following the conditions below:
2D Finite Element modelling
2 testing lines in parallel (tested and reference element)
CFC_NB31 following the dimensions in appendix 1
No linear model i.e. thermal properties = f (temperature)
Cooling phase
Meshing of flaw = void (thickness 0.3mm)
Surface natural convection
3 flaw positions φ (0°, 45°, 90°) and 1 flaw extension Dφ(60°)

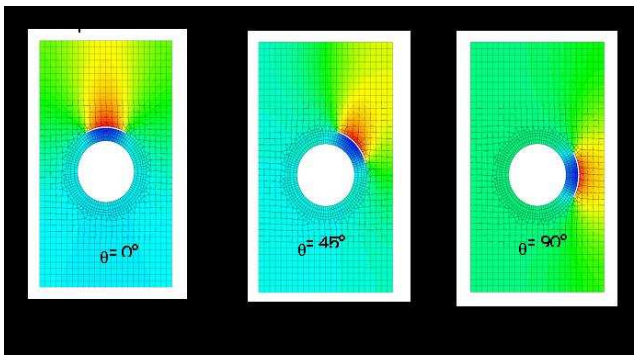

Figure 2: FE calculation for a flaw extension Δθ=60°at different position (DTref max)

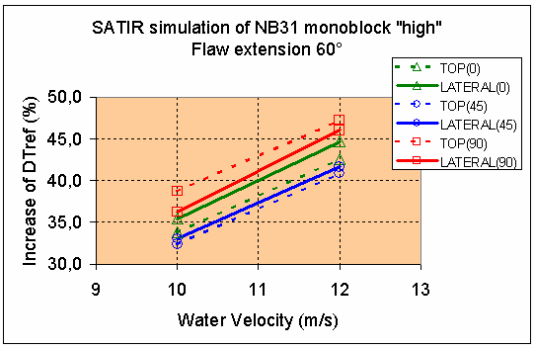

Figure 3: Improvement of DTref the water velocity

The figure 3 illustrates the improvement of the DTref value versus the evolution of the SATIR water flow rate. In figure 3, one can expect a significant increase of performances with a water flow improvement. Besides calculations show also the need to check the monoblock elements on the 2 observation surfaces (top and lateral surface).

This will lead to a more accurate detection of the defect position.
- 47% of improvement with a water velocity of 12m/s in each element (global flow rate 10m^3/h),
- 38% of improvement with a water velocity of 10m/s in each element (global flow rate 8m^3/h).

MINIMISE THE TEST TIME REQUIRED

The calculation of the heat transfer convective coefficient during the heating and cooling cycle following the Dittus-Boelter correlation highlighted that the water dynamic viscosity played a significant role on the sensitivity of detection.
The figure 4 shows the effect of the heat transfer coefficient difference on SATIR DTref value between the heating cycle (h100°C =30000W/m.°C) and the cooling cycle (h5°C =13000W/m.°C).
The figure 5 presents similar DTref values using a constant heat transfer coefficient (h mean=20000W/m°C) for both heating and cooling cycle. This demonstrates that the advisable choice of the cooling cycle leads to an improvement of the detection sensitivity.

The SATIR process would be also significantly simplified using only one cycle.

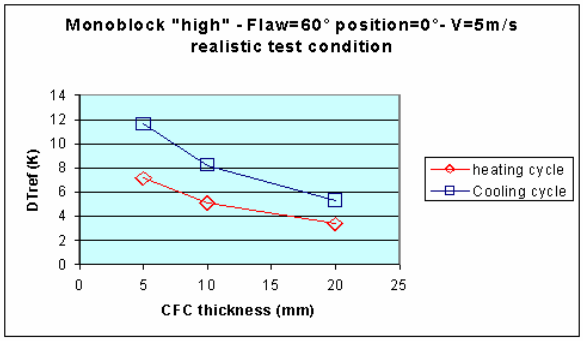

Figure 4: Sensitivity effect following the heat transfer coefficient

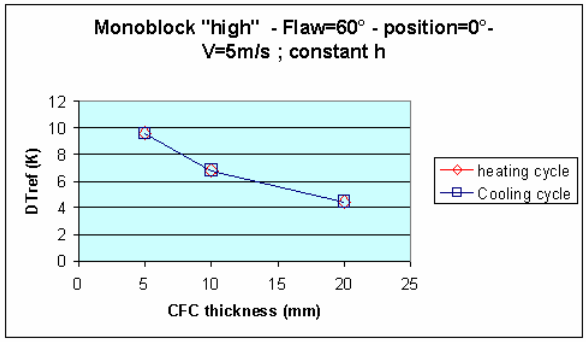

Figure 5: Constant heat transfer coefficient during heating and cooling cycle

To validate the previous calculations, experimental SATIR tests on Vertical Target Full Scale - CFC part (thickness = 5mm) – have been performed; it pointed out clearly a better sensitivity during cooling cycle up to 20% (figure 6).

The retained solution will take into account only the cooling cycle instead of the three pulses usually used.

This test bed operation mode involves:
A reduction of the film size (750 Mb to ~400Mb),
A shortening of the data processing time (by 2/3).

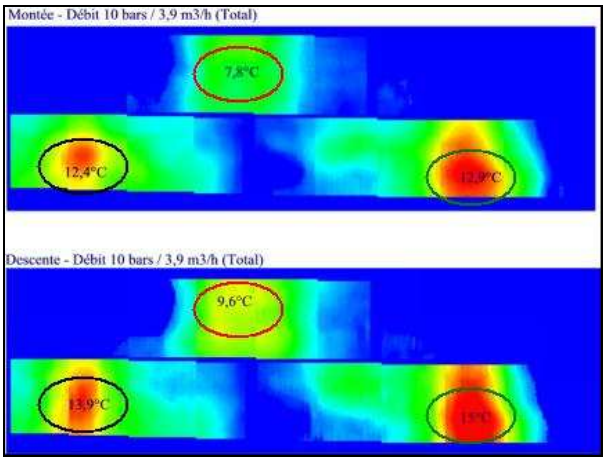

Figure 6: Infrared DTref cartography: Experimental demonstration of better detection sensibility during the cooling cycle

PROPOSED IMPROVEMENT CONCEPT

SATIR is going to be transformed into two independent injection lines, a hot and a cold one, synchronized by an industrial programmable logic controller. For comparison, the present SATIR equipment has a single injection stage shared by the 2 water sources (see figure 7).

This new SATIR ITER concept is based on two continuously operated pressurized stages. Each injection stage is designed to be operated all day long under pressure with the steepest switching injection time in the mocks-up, typically <= 1 s (measured on the flow rate edge).

This concept is already implementation of the W7X HP prototype stage designed for the Wendelstein mocks-up in 2004. It has been qualified during one year of IR testing on the W7X mocks-up and it is now fully in operation (figure 8).

Figure 8: The pumped and regulated loop

However present SATIR had to be upgraded during the phase 1 of this contract (Sept-Dec 2005) to improve two mains features of the test bed:

To supply enough flow for the two fluid sources in order to reach the ITER maximum requirements. This was done by an increase of pipes diameter.

To enhance the hot source availability: operation is now done at 100°C with a maximum re-heating time of 2 hours from ambient temperature to 100°C. The capacity of the new hot source would allow 4 successive ITER tests without re-heating but it's normally re-heating on line between two tests within a time duration of 12min. The total volume is VT=1200 L.

A more powerful pump will be dedicated to the cold injection stage and supplying the following parameters: 6<Q<10 m^3/h, 5<P<12b, P, Q Injection regulated, Out of shot flow rate regulated (Q By-pass) to be more rapid to switch into test mode, Response time <=1 s (pump + variable speed controller).

Operation at such a high flow rate involves several consequences, which make part of the test bed reliability enhancement:

First of all, it is indispensable to prevent the heating source from depressurization otherwise the water heaters may run into a boiling phase. That's the reason why a safety device is installed between the water buffer tank and the two water sources: the feeding pump which has the role of maintaining a constant pressure in the network at the input of the water sources. The specification of feeding pump is the following:

P_{in}= atmospheric pressure, P_{out}=5b at Q nominal=10m^3/h,

It consists of 2 parallel pumps with a variable speed controller on each one, plus 2 series bladder tanks.

Secondly, SATIR diagnostic has to be freed from the pressure fluctuations induced by the Cadarache open loop water network (up to 20% fluctuations). This is the function of the water buffer tank, which has the following specification:
An available volume of VA=3250L, a total volume of VT=3750L, A regulated water level by a radar probe, and a refilling time of TR=18min, compatible with TORE SUPRA network.

Thirdly, implementation of two independent HP stages is now necessary. This will protect the present unique pump against the repetitive thermal shocks which might degrade its reliability even with q max pump=120°C. And in the end, as the devices to control are becoming quite numerous, a new command control system has to be developed, based on an industrial programmable logic controller with a graphic interface.

CONCLUSIONS

SATIR diagnostic has been identified as the basic test to decide upon the final acceptance of the Divertor PFCs. In order to check the ITER components, the possibility to increase the defect detection sensitivity of SATIR has been investigated. The retained solution [1] is to increase the water velocity inside the tested component to improve the heat transfer convective coefficient. Finite element calculations, performed on the CFC monoblock, showed that this water velocity increase would improve in a significant way, the sensitivity of SATIR diagnostic: 47% of DTref improvement with a water velocity of 12m/s in each element, corresponding to 10m^3/h of global flow rate. These calculations also pointed out the interest of checking the elements on both top and lateral surface in order to locate more accurately the defect position.

Calculations also show a significant effect of the heat transfer coefficient difference on SATIR DTref value between the heating and the cooling cycle. Besides, operation with only one cycle – the most sensitive one- will minimise the requested time to check the Divertor PFCs. The SATIR process would be significantly simplified using only one cooling cycle.
These simulations of SATIR test allowed to design an upgraded SATIR facility taking into account the technical requirements of ITER mock-ups for the final acceptance of the Divertor PFCs.

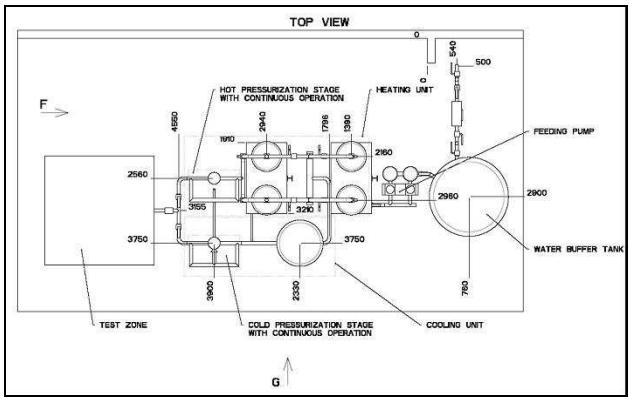

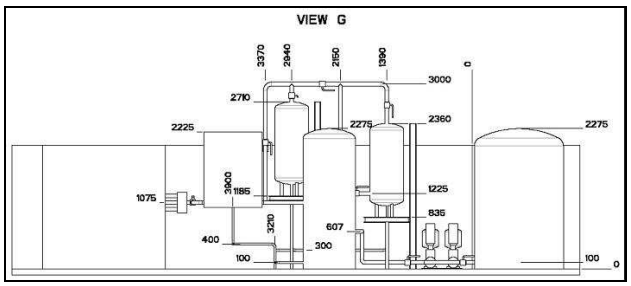

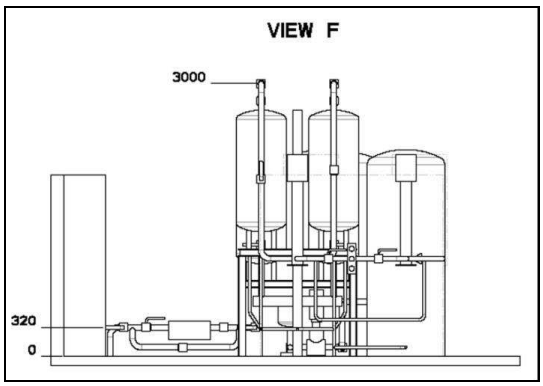

Figure 7: Drawings of the system

REFERENCES

[1] "Improvement evaluation for infrared detection of PFC flaws" Final report CEFDA 00-565

[2] "Development of an original active thermography method adapted to ITER plasma facing components control" Fusion Engineering and Design 75-79 (2005) 401-405

[3] EFDA Meeting report at CEA Cadarache octobre, 11th, 2005

TASK LEADER

Alain DUROCHER

DSM/DRFC/SIPP/GCFP
CEA-Cadarache
F-13108 Saint-Paul-lez-Durance Cedex

Tel. : 33 4 42 25 62 69
Fax : 33 4 42 25 49 90

e-mail : alain.durocher@cea.fr

CEFDA05-1248

Task Title: TW5-TVD-ACCEPT: INFLUENCE OF THE CARBON EROSION ON THE ACCEPTANCE CRITERIA OF THE ITER DIVERTOR

INTRODUCTION

This study deals with erosion calculations of CFC (Carbon Fibre Composite) monoblocks of the ITER divertor vertical target. These monoblocks must sustain high heat fluxes of 10 MW/m^2 during 1000 s (normal operation) and 20 MW/m^2 during 10 s (off-normal event).
One can expect erosion instability in normal operation in case of one faulty monoblock besides good ones due to the balanced rate between the various erosion mechanisms at different temperatures [3],[5]. Coherent plasma parameters, which represent the worst cases of erosion in normal operation, have been taken into account to analyse the erosion behaviour of the monoblocks, the aim of the study being to evaluate the eventual impact of these phenomena on the acceptance of the monoblocks (the monoblocks are considered thermo-mechanically compliant to a defect but this compliancy could be drastically reduced by erosion instability).
It was shown that a 20% decrease of CFC conductivity or a defect at the CFC/Cu bond affects seriously the erosion rate and thus temperature distribution. However this erosion instability seems to be not critical in case of 20 MW/m^2 during 10 s.

CALCULATION CONDITIONS

The used model for calculation is composed of one monoblock between two half-monoblocks (figure 1).The calculations are performed in 2D.
According to B2-EIRENE calculations, the total power load for normal operation of ITER on the outer vertical target consists of about 30% due to irradiation from the plasma and 70% due to particles in glancing incidence (see figure 2 the power distribution along the target).

An increase of the power load corresponds to an increase of the density and plasma temperature and leads to a shift of the maximum to the separatrix near which temperature and erosion instabilities are possible.
It has to be noticed that physical erosion increases with plasma temperature (particle energy), deuterium particle fluence, angle of incidence and surface roughness, whereas chemical erosion depends on plasma temperature (ion energy), CFC temperature, deuterium particle flux and surface roughness.
Operation regimes where instabilities are possible correspond to a power load of about 3~6 MW/m^2.
Nine cases have been recognized as having a potential risk of erosion instability (figure 2) and table 1.

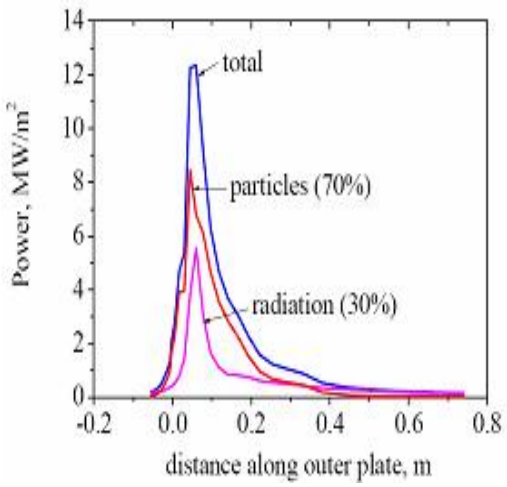

Figure 2: Power load distribution along the outer plate and table of selected cases

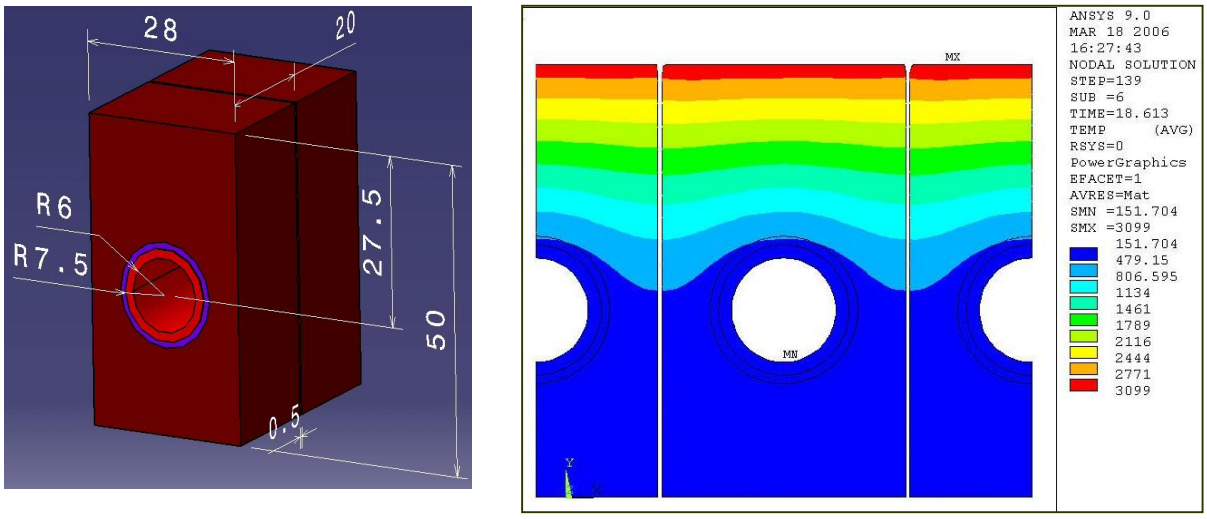

Figure 1: Geometry of one monoblock and example of FE calculation

Table 1: 9 selected cases

Case *(location on the target)*	**Power load (MW/m²) 70% from glancing inc. 30% from normal inc.**	**Ion flux (D/m²)**	Te Plasma temperature (eV)	**E_0 = 6.Te**
1	**2.8 || 1.2**	**1E+23**	5	**30**
2	**2.8 || 1.2**	**5E+22**	20	**120**
3 (*x= 0.140)*	**2.31 || 0.99**	**7.4E+22**	20	**120**
4 (*x= 0.117)*	**3.25 || 1.4**	**9.4E+22**	19	**114**
5 (*x= 0.165)*	**1.75 || 0.75**	**5.7E+22**	15	**90**
6 (*x= 0.117)*	**4.2 || 1.8**	**9E+23**	1	**6**
7	**3.22 || 1.38**	**1E+23**	16	**96**
8	**2.8 || 1.2**	**3E+24**	1	**6**
9	**4.2 || 1.8**	**9E+22**	18	**108**

Due to the rather low heat flux load (< 5MW/m^2) there is no sublimation for these cases.
For each case 3 runs can be performed:
a) Standard value of conductivity and no defect
b) Conductivity reduced of 20% for the central monoblock
c) Defect of 90° at the CFC/Cu interface located at -30° (the glancing incidence being 3°)

Boundary conditions
The power load is applied on the upper part (with eventual penetration into the gaps). Forced convection in subcooled boiling is applied at the cooling tube inner surface. And cyclic boundary conditions are applied on the 2 half monoblocks (left and right sides are forced to have the same temperature distribution).

ANSYS CALCULATIONS

Modelling and calculations
The modelling has been developed by the ITER team. It is based on the refinement of the mesh at the upper surface of the monoblocks (typically 9-13 µm x 100 µm) and the killing of cell when the erosion reaches the volume of one cell. In addition to development of routines that calculate chemical [1] and physical [2] and sublimation erosion an important development was made to take into account angle of incidence and shadowing effects. The calculation is a transient one and improvements to the code were done by ITER all along the calculations in 2006 [3], [4], [5], [6].

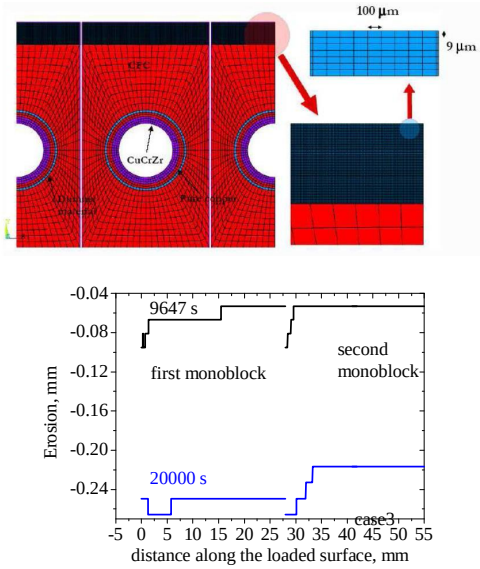

Figure 3: Modelling in ANSYS a typical result (Case 3b)

Results and conclusions of the ANSYS calculations
The cases 1, 2 and 3 have been calculated with ANSYS in the hypothesis b and c (left and right location of defects have been investigated). The completed results are given in [6].
The main comments are the following:

- The variation in the thermal conductivity of two neighbour monoblocks by 20% does not exceed the difference in erosion in 20-40 µm that is about 0.1-0.2% of total CFC thickness.

- This difference between erosion of two neighbour monoblocks can slightly be increased or be decreased with time but is not a critical point in normal operation (the calculations have been done up to 50 plasma discharges without taking into account ELMs, transient and disruptions which, probably, will depress the chemical erosion by increasing the surface temperature and, consequently, depress the instability).

- The effect of ELMs and off-normal events should be taken into account for the future investigation.

- The influence of a defect of maximum available size of 90° (located at -30° and with an extension of 90°) in the joint area between CFC and cooling tube on erosion and temperature instabilities is less pronounced compared to the difference in thermal conductivities of neighbour monoblocks.

- Effect of deeper edge erosion of less eroded monoblock has been observed. Such effect takes place only in the case of different thermal conductivities of two neighbour monoblocks.

Consequently, on the point of view of erosion instability, the presence of a defect in the joint area between CFC armour and cooling tube of size of 90° and a reduction of the thermal conductivity by 20% of one the neighbour monoblocks are acceptable for the present design and operation conditions.

Difficulties encountered running the ANSYS model
The main difficulty encountered with these transient calculations is the refinement of the mesh, which leads to very long computation and reduce the possibility to run many cases (for example to calculate the erosion of 100-200 µm, the computer time of 5-7 days was necessary).

It is also important to notice that the time step can have an influence and that the technique of rectangular fine cells may increase artificially the surface in contact with the plasma.

CAST3M CALCULATIONS

All the cases have been calculated for 10 000s simulation, roughly 25 ITER pulses.
The CASTEM calculations were undertaken to crosscheck the ANSYS calculations using another methodology. The calculations is based on a series of steady states the mesh being updated at each step of the iterations. The model was developed thanks to the routines developed 10 years ago for the toroidal pump limiter of Tore Supra and takes into account penetration and shadowing effects [7].

CAST3M: calculation validation

Mainly chemical and physical erosion was validated against original equations and ANSYS calculations. Erosion calculated with CASTEM methodology is fully continuous and in agreement with analytical equations (figures 4 and 5) [7].

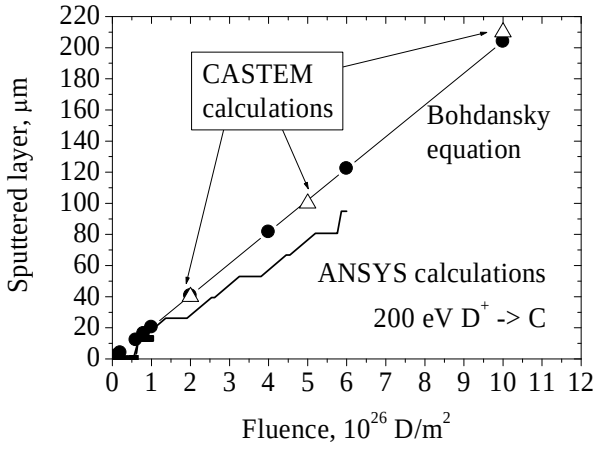

Figure 4: Physical sputtering with CAST3M

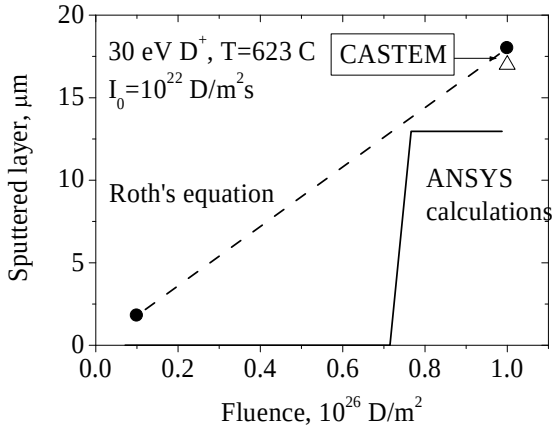

Figure 5: Chemical erosion with CAST3M

CAST3M calculation results

Calculations with CAST3M are very quick and very easy to performed. In these conditions the 27 (9x3) runs were performed up to 10000 s (= 25 pulses of 400 s) and 6 others (1a, 1b, 2a, 2b, 3a, 3b) were redone up to 40 000s (= 100 pulses) [8].

No dramatic erosion was found, however sensitive erosion differences between monoblocks have to be pointed out (see an example figure 6).

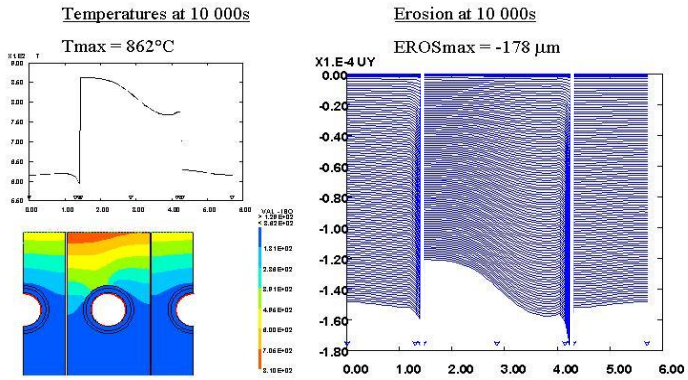

Figure 6: Case 2c: Temperature map at 10 000s and evolution of the erosion up to 10000s

COMPLEMENTARY CALCULATIONS WITH CAST3M

In order to check what could happen with this erosion instability it was decided to run one case with normal operation during 10 000 s and then to apply 20 MW/m^2 (70% conductive and 30% radiation) during 10 s. Such a result is given figure 7 below for case 8c: at the end of the 10 000 s the erosion is about 0.1 mm and it increases up to about 0.9 mm during the 10 s at 20 MW/m^2. To do such a calculation it was necessary to cancel the cyclic boundary conditions that are not appropriated here. One can observe on figure 7 an important erosion of the faulty central monoblock that leads to plasma shaping of the adjacent monoblock on the left.

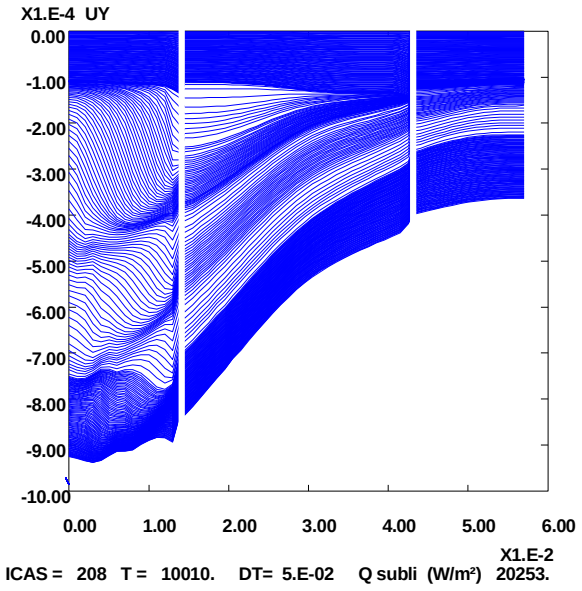

Figure 7: Case 8c: Evolution of the erosion during 10 s after 10000s of normal operation

CONCLUSIONS

This task demonstrated the capability to run erosion calculations with both ANSYS (transient calculation) and CAST3M (series of steady states). These calculations have pointed out some erosion instabilities for the studied cases (neighbour monoblock with reduced conductivity or with 90° defects) but that phenomenon can be considered not critical up to now.
Further investigation of critical cases should be pursued since one has now the tools for such calculations.
As a consequence no modification of the acceptance criteria of the monoblocks is foreseen.

REFERENCES

[1] J. Roth, "Chemical erosion of carbon based materials in fusion device". Journal of Fusion Materials, 266-269 (1999), pp. 51-57

[2] J. Bohdansky. "A universal relation for the sputtering yield of monatomic solids at normal ion incidence". Nucl. Inst. and Meth., B 2:587, (1984)

[3] *E. D'Agata, R. Tivey*, "Towards the development of workable acceptance criteria for the divertor CFC monoblock armour". Fusion Engineering and Design 75-79 (2005). pp. 441-445

[4] E. D'Agata, O. Ogorodnikova, R. Tivey, C. Lowry, J. Schlosser, A program to Evaluate the Erosion on the CFC tiles of the ITER Divertor, SOFT, 2006

REPORTS AND PUBLICATIONS

[5] S. Fouquet, Influence of the carbon erosion on the acceptance criteria of the ITER divertor, INTERIM REPORT 1: ANSYS model for erosion simulation, CFP/NTT-2005.013

[6] O. V. Ogorodnikova, Influence of the carbon erosion on the acceptance criteria of the ITER divertor, INTERIM REPORT 2, Operation regimes of erosion and temperature instabilities, CFP/NTT-2007.003, (2007)

[7] J. Schlosser, Influence of the carbon erosion on the acceptance criteria of the ITER divertor, INTERIM REPORT 3: Modelling with CAST3M, CFP/NTT-2007.001 (2007)

[8] J. Bouvet, J. Schlosser, Influence of the carbon erosion on the acceptance criteria of the ITER divertor, INTERIM REPORT 4: Finite Element calculation results using CAST3M, CFP/NTT-2007.002 (2007)

[9] O. V. Ogorodnikova, Influence of the carbon erosion on the acceptance criteria of the ITER divertor, INTERIM REPORT 5: ANSYS calculations, CFP/NTT-2007.004 (2007)

TASK LEADER

Jacques SCHLOSSER

DSM/DRFC/SIPP
CEA-Cadarache
F-13108 Saint-Paul-lez-Durance Cedex

Tel. : 33 4 42 25 25 44
Fax : 33 4 42 25 49 90

e-mail : jacques.schlosser@cea.fr

Not available on line

Not available on line

Not available on line

Not available on line

Not available on line

CEFDA06-1372

Task Title: TW5-TVD-FABCON: DEVELOPMENT OF FABRICATION CONTROL METHODS FOR THE ITER DIVERTOR

INTRODUCTION

In the plasma facing components (PFCs), the failure of the heat sink to armour joints will compromise the performance of the Divertor and ultimately result in its failure and the shut down of the ITER machine.
In view of the procurement of the ITER Divertor, the development of non-destructive testing (NDT) of the heat sink to armour joints is an essential topic to be addressed. NDT techniques will also be used to assess the quality of the plasma facing components PFCs and their acceptability in the ITER machine.
An infrared thermography test bed named SATIR (Station d' Acquisition et de Traitement InfraRouge) has been developed by CEA in order to evaluate the manufacturing process quality of actively water-cooled plasma facing components (PFCs) before their installation in TORE SUPRA. The infrared thermography allows to characterize the bond between CFC armour tile and metallic heat sink and is becoming more and more a valuable tool for detecting cracks and failures. It is a complementary and necessary non-destructive testing method to the ultrasonic examinations and gives a global information about the soundness of the heat path thus being a fast and economical way to assess the acceptability of a CFC armoured component prior to its installation into a fusion machine. Within the on-going work on acceptance criteria, which is being carried out by EU and the ITER International team, SATIR inspection has been identified as the basis test to decide upon the final acceptance of the Divertor PFCs.
In order to improve the defect detection capability of the SATIR test bed, the possibility of merging the infrared test data with the ultrasonic test data has been identified. A cross analysis of these 2 techniques promises to provide a more accurate and reliable sizing and location of the defects.
This study was carried out on 3 CFC monoblocks (#6, #8, #15) with calibrated defects (θ,dθ) and allowed to set up the data merging tools. This work will be extended in 2007 when SATIR is operational.

2006 ACTIVITIES

MONOBLOCKS CFC DESCRIPTION

The Divertor is one of the most challenging components of the next step ITER machine. The PFCs are actively cooled thermal shields devoted to sustain the heat and particle fluxes during normal and transient operations as well as during disruption events. In the PFCs, the failure of the heat sink to armour joints will compromise the performance of the Divertor and ultimately result in its failure and the shut down of the ITER machine. There are tens of thousands of such joints in the Divertor assembly, either carbon fibre composite (CFC) to copper alloy (CuCrZr) joints or tungsten (W) to CuCrZr joints (Figures 1 and 2).

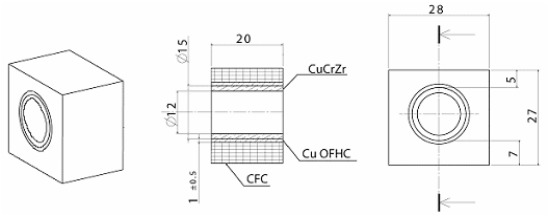

Figure 1: CFC monoblock sample"short"

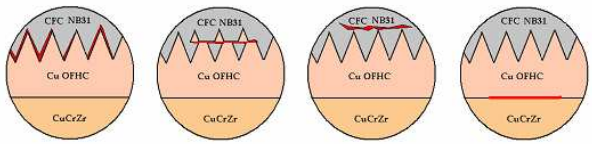

Figure 2: Assembling defects encountered during the PFC manufacturing

INFRARED THERMOGRAPHY METHOD (SATIR)

The SATIR technique (French acronym for Infra Red Acquisition and Data Processing device) consists in recording the surface temperature evolution of the tested component with an infrared device during the circulation of a hot and cold-water front into the cooling channel of the component (figures 3 and 4). The transient thermal response is recorded and compared with those of a reference element [1]; the maximum of the temperature difference (criteria called DTref max) is stored for each armour tile. A bonding defect between heat sink and armour tile will be detected by a high value of DTref max. The result is a DTref value mapping of each surface expressed in a Cartesian reference (figure 5).

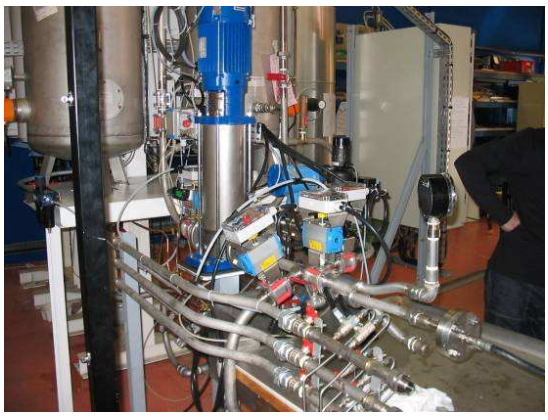

Figure 3: View of SATIR test bed (water injection stage)

SATIR test results:

Figure 4: CFC Monoblocks testing

- The mock-up 6 without defect (as reference)
- The mock-up 8 with a defect 0_65
- The mock-up 15 with a defect 45_35

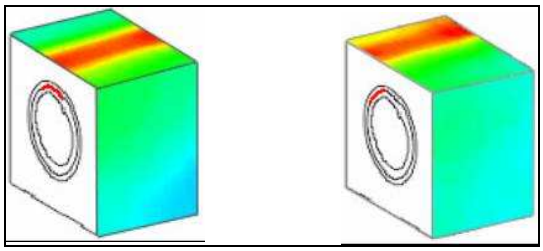

Figure 5: DTref map of mock-up_8 and DTref map of mock-up _15

ULTRASOUND TEST METHOD

The ultrasonic tests are based on the reflection of ultrasound mechanical waves emitted through a material to be tested. The intrinsic porosity of the CFC makes difficult a classic ultrasound test.

The test is performed from each monoblock cooling channel (filled with water). The mechanical waves are reflected on a mobile mirror (45°). The waves are only focused in the acoustic impedance of one interface, either CFC-Cu or Cu-CuCrZr.

The transducer and the mirror works in translation and in rotation inside the tube, the obtained cartography is expressed in a cylindrical reference (figure 6).

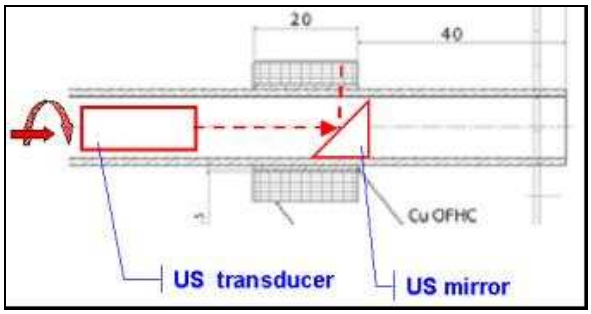

Figure 6: Ultrasound device

One can note that this test is not functional contrary to the SATIR test: the cartography gives the acoustic impedance of the interfaces, not its thermal properties. Furthermore, the ultrasound test being focused in the interfaces, it does not detect the possible presence of defects in the CFC armour.

Ultrasound test results:

CIEMAT association [2] supplied the US results (figure 7). The results represent a percentage of reflection of the ultrasound signal (in dB unit). The displacement resolution of the US probe is 1mm; the angular resolution is 1°, what gives thus 7200 measures for the monoblock (depth of 20mm).

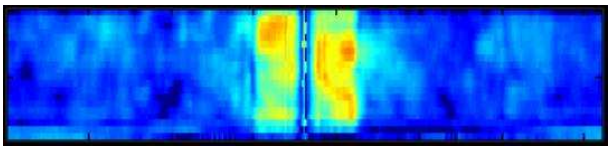

Figure 7: Ultrasound results of mock-up_8

One can note on the figure 7 a discontinuity (impedance) in the center of the defect, which corresponds to the drilling in the copper necessary of the defect electro-erosion machining.

The orthotropic geometrical projection

To combine the US data with the infrared SATIR data, one can use the geometrical projection (figure 8). The purpose being to transpose US values expressed in a cylindrical reference (θ,y) in a Cartesian reference (x, y).

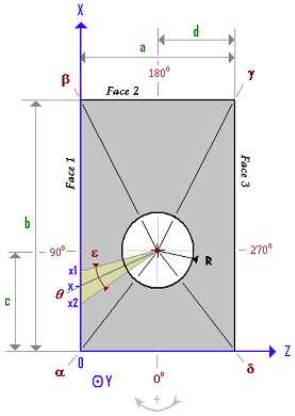

Short Monobloc
a = 28 mm
b = 27 mm
c = 14.5 mm
d = 14 mm
R = 8.5 mm
α = 43.9°
β = 131.8°
γ = 228.2°
δ = 316.0°

Figure 8: Geometric projection

The geometrical projection is a radial projection on the 3 faces by means of usual trigonometric formulae. The major drawback of the geometrical projection is the absence of physical meaning of the method.

The orthotropic effect of the NB31 involves a modification of the temperature field on the surface of mock-up during the SATIR test. To combine the US results with the SATIR tests, it is necessary that the geometrical projection considers the ratio of orthotropy because the pixel-by-pixel fusion requires a spatial coherence (figure 9). For that purpose, a shape factor was applied to the geometry of the monoblock before the pixel projection.

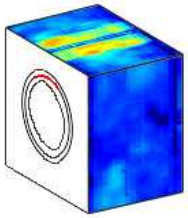

Figure 9: US geometric projection results

The ANSYS thermal projection

The thermal projection of the US data was performed using ANSYS finite element model (figure 10). The US cartography is implemented in the model at the ad-hoc interface CFC/Cu. The result is a SATIR like DTref mapping being directly combined with SATIR experimental data (figure 11).

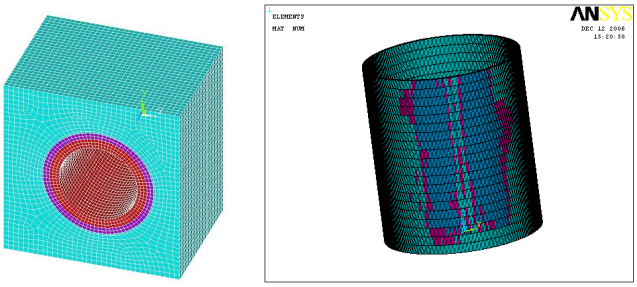

Figure 10: ANSYS Model of short monoblock and CFC/Cu interface with implemented ultrasonic signals

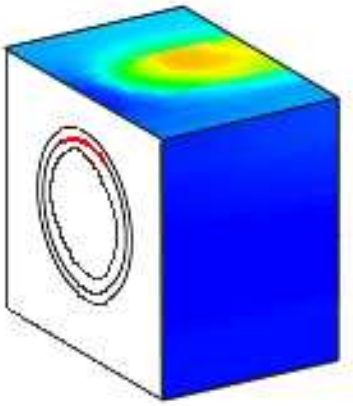

Figure 11: US thermal projection results after data processing

PRINCIPLE OF THE DATA MERGING

A data-merging module has been developed with the aim to improve the confidence on the measurement. The concept of data merging was developed in order to offer user-friendly machine interfaces and give decision capacities to non-experts in complex multi-sensor environments. This study aims at the coupling of the two methods of infrared thermal imaging previously mentioned. The data marging method is based on the theory of evidence, which was defined by Shafer based on the work of Dempster on the generalization of the theory for the management of uncertainty and ignorance [3], [4]. This method assigns degrees of confidence, so called "sets of masses" to simple hypotheses, or combination of simple hypotheses for each NDT. Afterwards the merging of the experimental knowledge provided from different NDT images is performed through the Dempster orthogonal summation rule (1).

$$m(H) = m_1 \oplus m_2(H) = \frac{\sum_{H_i \cap H_j = H} m_1(H_i).m_2(H_j)}{1-K} \quad (1)$$

This method has the advantage to be adapted to the concept of decision thresholds used in the domain of non-destructive inspection [5], [6]. Firstly a pixel-by-pixel merged method, which is more demanding than relative repositioning of the two NDT images, was chosen. Secondly the probabilities on hypotheses accuracy, needful for the Dempster-Shafer method, were defined for each NDT. This requires a far-reaching experimental training. In our application, the hypothesis H1 corresponds to the presence of defect; the hypothesis H2 characterizes the absence of defect; and the hypothesis H3 corresponds to the ignorance. For each measurement, thresholds were established based on whether the pixel will be classified as defective, or not defective or ignorance (figure 12).

From 2 thresholds (C1 and C2) 3 zones are defined by NDT, which represent the regions where the decision is one of the 3 hypotheses H1, H2 or H3 with a certainty, which will be weighted by the sets of masses (to balance the importance of hypotheses): $m_n(H_i)$. If the transitions between zones are used alone, the decision changes are very abrupt and will be too sensitive to measurement noise.

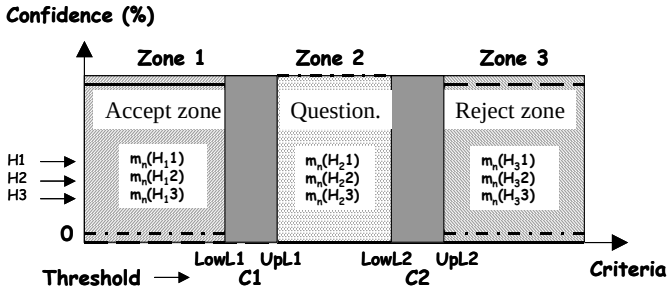

Figure 12: Definition of zone limits and associated hypotheses for n NDT

To obtain a more continuous behaviour from the transitions, fuzzy logic functions are used. Lower (lowL) and upper (UpL) limits then need to be defined for each zone. The purpose is to calculate the sets of masses after combination of the sources for each hypothesis. The combining of 2 or more NDT allows to increase the confidence of defect detection by reducing the uncertainties. It is also necessary to introduce the conflict term K (2) between the NDT sources when they are contradictory. For example, if the sets of masses involve a strong confidence in the measurements and that the portion of hypotheses H3 (ignorance) is weak, then the conflict term K increases.

$$K = \sum_{H_i \cap H_j = \emptyset} m_1(H_i) m_2(H_j) \quad (2)$$

Data merging results

The feasibility was demonstrated on mock-up_8 provided by Plansee manufacturer.

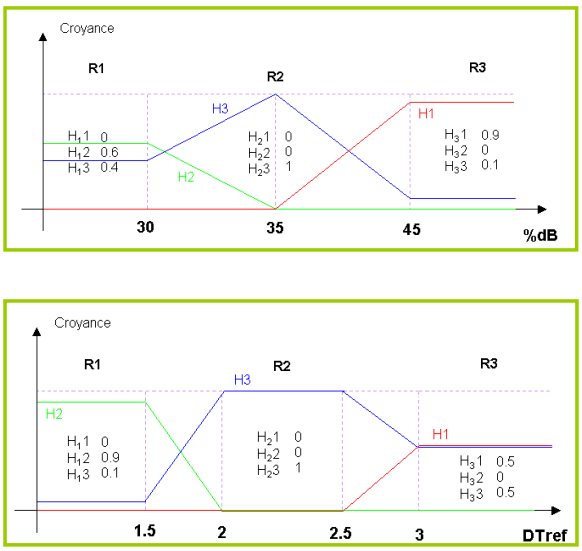

Figure 13: Zone limits and associated hypotheses for SATIR (DTref) and US (%dB) NDT

1) Definition of hypothesis sets of masses, thresholds for each NDT (figure 13). A next step in 2007 based on a statistical experimental study will allow to optimise these inputs.

2) Data merging procedure highlighted 2 interesting cartographies: the cartography of presence of defect H1 and the cartography of conflict K. H1 cartography increases the confidence in the defect presence. The cartography of conflict K represents the contradictions between the merged data:

- Zones of thermal diffusivity around the defects
- The presence of defects in the CFC (conflict cartography)

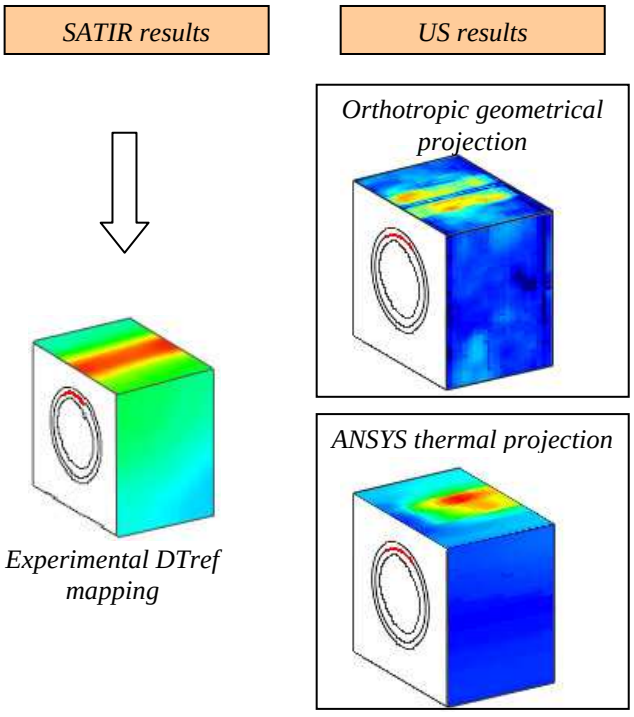

Figure 14: SATIR and US cartographies of mock-up_8

As expected the data merging of mock-up_8 shows a central defect presence of 100%. In the case of calibrated defects, the defect machining involves an ultrasonic artefact in the analysis of H1 cartography, which won't appear with real defects. In spite of a bad precision of the thermal projection, the tools which were set up during this feasibility step are operational. Finally the data merging of DTref SATIR and orthotropic geometrical projection presents the best relevance (figures 14 and 15).

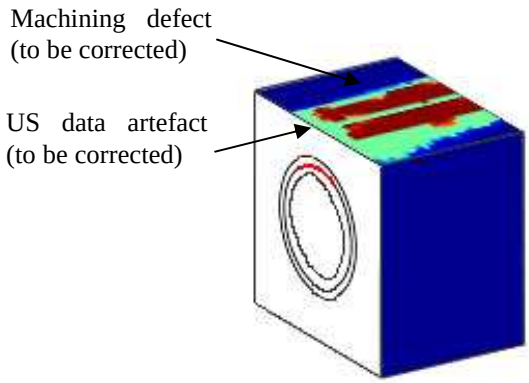

Figure 15: Cartography of defect presence (H1) for mock-up_8(0_65°)

CONCLUSIONS

The US data are not directly able to be merged with the SATIR data results; this study consisted to set up a method and tools making possible the US/IR data merging. Two methods were developed to merge the US and SATIR data: the orthotropic geometrical projection and the ANSYS thermal projection. The geometrical projection is more effective than the thermal projection: faster, simpler, and more accurate. However the thermal projection is not really optimised and its interest is not still quantifiable.

During this intermediate step, only 2 CFC monoblocks with calibrated defects were tested on SATIR test bed. Even if the reference monoblock used on SATIR presented a real asymmetrical defect, these preliminary results are very encouraging. In this framework it'll still remain to determine in 2007 the ultrasonic merging parameters: sets of masses, hypothesis and thresholds. The SATIR and US merging data on real manufacturing defects will show the power of this method. One can summarize this preliminary step by: a method and operational tools exist now; it remains to optimise it in 2007 using all the CFC monoblocks.

REFERENCES

[1] A. Durocher et al., Development of an original active thermography method adapted to ITER plasma facing components control, Fusion Engineering and Design, 2005, 75-79:401-405

[2] M.Garcia, Ultrasonic inspection of the CFC monoblocks mock-ups manufactured by Plansee, code IN-IT-DIV 002 (Dec.2006) CIEMAT document

[3] J. Esteban, A. Starr, R.Willets, P. Hannah, P. Bryanston-Cross, A review of data fusion models and architectures: towards engineering guidelines, Neural Comput. & Applic. , 2005,14:273-281

[4] D. Horn, W.RR. Mayo, NDE reliability gains from combining eddy-current and ultrasonic testing, NDT&E International, 2000, 33: 351-362

[5] A. Durocher, J. Moysan, F. Escourbiac, M. Missirlian, N. Vignal, Data Merging of Infrared Images for Plasma Facing Components Inspection, to be published in Fusion Engineering and Design 2006

[6] J. Moysan, A. Durocher, C. Gueudré, G. Corneloup, Improvement of the Non-Destructive Evaluation of Plasma Facing Components by Data Combination of Infrared Thermal Images, NDT&E Int.

TASK LEADER

Alain DUROCHER

DSM/DRFC/SIPP/GCFP
CEA-Cadarache
F-13108 Saint-Paul-lez-Durance Cedex

Tel. : 33 4 42 25 62 69
Fax : 33 4 42 25 49 90

e-mail : alain.durocher@cea.fr

CEFDA06-1373

Task Title: TW6-TVD-ACCREV: DEFINITION OF ACCEPTANCE CRITERIA FOR THE ITER DIVERTOR

INTRODUCTION

As far as the plasma facing components (PFC) of ITER are concerned, the failure of the heat sink to armour joints will compromise the performance of the machine. There are tens of thousands of such joints in the Divertor assembly, either carbon fibre composite (CFC) to copper alloy (CuCrZr) joints or tungsten (W) to CuCrZr joints. In preparation for writing the procurement specification for the ITER divertor PFC, this task is undertaken with the objective of defining workable acceptance criteria for the PFC armour joints. Investigations of possible detection of the occurrence of the Critical Heat Flux via acoustic emission are also developped in this task.

2006 ACTIVITIES

ACOUSTIC EMISSION

Acoustic signals from piezoelectric sensors (accelerometers 0–40 kHz and microphone 100-400 kHz) were recorded during a Critical Heat Flux (CHF) test performed at FE200 facility on a medium-scale ITER Divertor vertical target mock-up so-called HRP [1]. Design of the mock-up (W and CFC monoblocks with twisted tape insert), thermal and hydraulics testing conditions (50°C, 3.5 MPa, 12m/s) were considered as relevant to ITER conditions

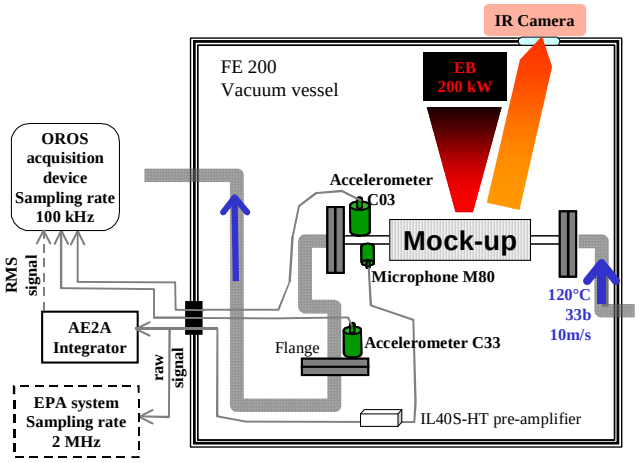

Figure 1: Mock-up setup and instrumentation

The evolution of the signals presented on figure 2 are consistent with the boiling process. In particular, the increasing of the acoustic emission energy (M80 sensor) during the development of partial boiling, then the decreasing and the plateau of vibration energy (C03 & C33 sensor) disclosing the presence of the fully boiling regime.

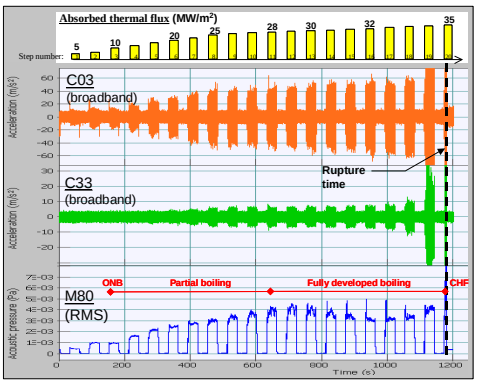

Figure 2: Acoustic signal during increasing flux steps, up to rupture at 35 MW/m²

This is explained by the fact that during the fully developped boiling regime the bubbles detach from the heated channel surface and collapse (condensation) in the bulk fluid rather than on the heated surface in the case of partial sub-nucleate boiling, consequently the acoustic shock waves propagation is less efficient, even if the number and size of bubbles increases. This decreasing of acoustic energy level can be considered as precursory indicator of CHF.
Further data processing pointed out other potential precursory indicators of CHF:

- Vibration level: increase of global RMS level (broadband) or restricted to a band limited (occurence of a high vibration peak at 680 Hz);

- Vibration envelope level: low frequency modulations of HF vibrations, calculated on the Hilbert envelope;

- Vibration statistical indicators: decrease of Skewness, Kurtosis and Crest factor.

The remote sensor (C33 accelerometer, 2 meters down) was sensitive to the acoustic phenomena, it was found by cross correlation with the C03 sensor that this is due to the fact that the acoustic waves propagate mainly into the fluid. This is promising for a future operational system where the sensors cannot be located near the in-situ component.

HIGH HEAT FLUX TESTING

In the frame of this task, it is planned to perform fatigue testing of 108 samples with artificial defects. In 2006, 14 Tungsten (W) flat tile samples were manufactured via brazing technique onto a CuCrZr heat sink with a compliant layer of soft Copper by Ansaldo Ricerche, some calibrated defects were prepared at the joints W/Copper and Copper/CuCrZr (figure 3).

These 14 samples was connected on a cooling system for FE200 testing tested at FE200 facility [2] (figure 4).

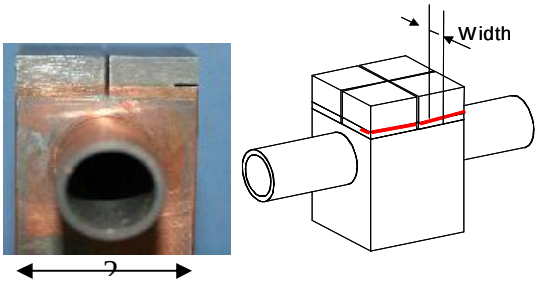

Figure 3: View of the elements and implementation of calibrated defects at the edge 2, 4 or 6 mm width, 0.3 mm thickness

Figure 4: Cooling system for FE200 testing with the 14 samples splitted into 2 x7

The testing steps are detailed in table 1, an infrared view of 7 elements is given figure 5. All the 4 mm and 6 mm defects were detected and stable during the fatigue. Further analysis taking into account the non destructive examination are running.

Table 1: Description of the testing steps

Testing steps (10 sec. ON / 10 sec. OFF)	Observations
5 MW/m² x 3000 cycles	No observed damage propagation
10 MW/m² x 500 cycles	No observed damage propagation

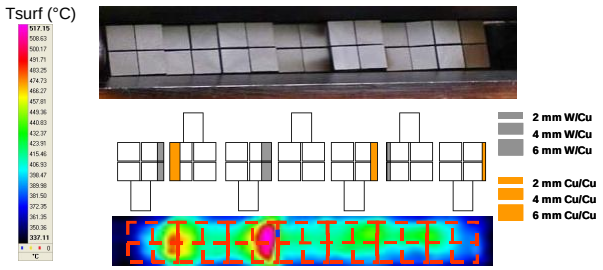

Figure 5: Infrared view of the 7 elements under a flux of 5 MW/m²

CONCLUSIONS

1) A study on acoustic emission demonstrated the consist of demonstrating this capability of detection in tokamak environment.

2) A first high heat flux testing campaign at FE200 facility on W flat tile samples with artificial defects demonstrated the detectability of 4 capability to detect precursory indicators of CHF with standard sensors and classical data processing techniques. A further step would and 6 m width defects and their stability under fatigue under fluxes up to 10 MW/m².

REFERENCES

[1] AREVA report NFT- F R-06.930A – CEA91 – EFDA/93-851JN – I.Bobin-Vastra, 2006

[2] Fus. Eng. Des. 75-79 (2005) 357-363, I. Bobin-Vastra, F.Escourbiac, M.Merola, P.Lorenzetto

TASK LEADER

Frédéric ESCOURBIAC

DSM/DRFC/SIPP
CEA-Cadarache
F-13108 Saint-Paul-lez-Durance Cedex

Tel. : 33 4 42 25 44 00
Fax : 33 4 42 25 49 90

e-mail : frederic.escourbiac@cea.fr

Not available on line

Not available on line

Not available on line

Not available on line

Not available on line

Not available on line